Scanning electron microscope-cathodoluminescence (SEM-CL) imaging of planar deformation features and tectonic deformation lamellae in quartz

M. F. HAMERS[*] and M. R. DRURY

Department of Earth Sciences, Faculty of Geosciences, Utrecht University, Budapestlaan 4, 3584 CD, Utrecht, The Netherlands

*Corresponding author. E-mail: hamers@geo.uu.nl

Abstract–Planar deformation features (PDFs) in quartz are essential proof for the correct identification of meteorite impact structures and related ejecta layers, but can be confused with tectonic deformation lamellae. The only completely reliable method to demonstrate the shock origin of suspected (sub-) planar microstructures, transmission electron microscope (TEM) observations, is costly and time consuming. We have used a cathodoluminescence (CL) detector attached to a scanning electron microscope (SEM) to image both PDFs and tectonic deformation lamellae in quartz to demonstrate the potential of a simple method to identify PDFs and define characteristics that allow their distinction from tectonic deformation lamellae. In both limited wavelength grayscale and composite color SEM-CL images, PDFs are easily identified. They are straight, narrow, well-defined features, whereas tectonic deformation lamellae are thicker, slightly curved, and there is often no clear boundary between lamella and host quartz. Composite color images reveal two types of CL behavior in PDFs: either they emit a red to infrared CL signal or they are nonluminescent. The color of the CL signal emitted by tectonic deformation lamellae ranges from blue to red. For comparison, we also imaged several shocked quartz grains at cryogenic temperature. In most cases, the PDF characteristics in cryo-CL images do not differ significantly from those in images recorded at room temperature. We conclude that SEM-CL imaging, especially when color composites are used, provides a promising, practical, low cost, and nondestructive method to distinguish between PDFs and tectonic lamellae, even when the simplest CL techniques available are used.

INTRODUCTION

Shock metamorphism in terrestrial minerals is diagnostic of meteorite impacts. The presence of shock-metamorphosed quartz, in particular, is essential for the correct identification of impact craters and distal ejecta layers. As quartz displays a wide array of shock features and is one of the most abundant and most stable minerals in the Earth's crust, shock metamorphism in quartz has been extensively studied in both natural and experimental settings (e.g., Engelhardt and Bertsch 1969; Kieffer et al. 1976; Goltrant et al. 1992; Gratz et al. 1992; Langenhorst 1994; Langenhorst and Deutsch 1994; Leroux et al. 1994; Stöffler and Langenhorst 1994; Grieve et al. 1996;

Trepmann and Spray 2005; Trepmann 2008). Shock features in quartz comprise mosaicism, planar fractures (PFs), planar deformation features (PDFs) or shock lamellae, high pressure polymorphs (coesite and stishovite), diaplectic glass, and lechatelierite. Recently, feather features (French et al. 2004; Poelchau and Kenkmann 2011) and ballen silica (Ferrière et al. 2009, 2010) have been proposed as additional shock indicators. PDFs are the most widely studied and most easily recognized shock features that form in quartz. They can be recognized as multiple sets of thin, very closely spaced (< 2 μm) sets of planar features that develop parallel to rational low index crystallographic planes, of which the most frequent orientations are (0001), $\{10\bar{1}3\}$ and $\{10\bar{1}2\}$

(e.g., Grieve et al. 1996). PDFs can be subdivided into nondecorated (fresh) and decorated (annealed) types. Fresh PDFs are thin, amorphous lamellae, whereas older structures are annealed or recrystallized, and can usually only be recognized as traces of microscopic fluid inclusions. PDFs parallel to (0001) are not amorphous lamellae, but mechanical Brazil twins (Goltrant et al. 1992), and unless they are annealed and decorated, they cannot be resolved in the optical microscope. Often multiple (max. 18) sets of PDFs develop in a single quartz grain, with the number of sets per grain increasing as a function of shock pressure. PDFs are usually penetrative through a whole grain, but do not cut across grain boundaries, fractures or planar fractures, unless these form at a later stage than the PDFs. A thorough review of shock metamorphic effects in quartz is given in Stöffler and Langenhorst (1994) and Grieve et al. (1996).

As PDFs are such important features of impact evidence, their correct identification is crucial. However, using a standard petrographic microscope, it can be difficult to distinguish between PDFs and nonshock-related planar microstructures in quartz. On several occasions, lamellar microstructures in quartz have been identified as PDFs, but have subsequently been disproved to be shock-related, or they remain controversial (e.g., Vrána 1987 versus Cordier et al. 1994; Surenian 1988 versus Leroux and Doukhan 1993; Ernstson and Fiebag 1992 versus Langenhorst and Deutsch 1996; Becker et al. 2004 versus Glikson 2004; Retallack et al. 1998 versus Langenhorst et al. 2005). Tectonic deformation lamellae, in particular, are often confused with PDFs, even though these two types of microstructure are fundamentally different in character. Tectonic deformation lamellae are more or less planar features that form in quartz grains as a result of comparatively slow, tectonic processes. When decorated with fluid inclusions, they are also known as Böhm lamellae (Böhm 1883; Christie and Raleigh 1959). Similar to PDFs, tectonic deformation lamellae are restricted to single grains and do not cross grain boundaries or fractures that formed before the lamellae. Tectonic deformation lamellae are often recognized in transmission electron microscopy (TEM) as slight misorientations in the crystal lattice; elongated, extremely narrow subgrains; arrays of fluid inclusions; subgrain walls; and zones of different dislocation density (White 1973; Drury 1993; Vernooij and Langenhorst 2005). Usually, a maximum of two sets develops in a sub-basal orientation (Drury 1993). Although recently, the term "Metamorphic Deformation Lamellae" was used in a review paper by French and Koeberl (2010), we will retain the term "tectonic deformation lamellae," which is more widely used in the literature. In general, tectonic lamellae are thicker, more widely spaced, and more curved than PDFs, but the two types of structure can be

remarkably similar in appearance in a light microscope (Fig. 1; see also for example Officer and Carter 1991; Lyons et al. 1993; Fig. 2c in Vernooij and Langenhorst (2005), or Fig. 29 and 30 in French and Koeberl (2010)). As a result of their apparent similarity, TEM observations of the microstructures are required to convincingly demonstrate the shock origin of lamellar microstructures in quartz (Leroux et al. 1994; Cordier and Gratz 1995; Vernooij and Langenhorst 2005). However, TEM analysis can only be done on very small sample volumes, is time consuming and costly, and TEM facilities are not easily accessible to many research groups. Scanning electron microscopy (SEM) observations, on the other hand, are quick, and nowadays many groups have access to an SEM instrument. Observations can be done on relatively large specimens, and standard polished thin sections can be handled without difficulties. This is a great advantage, as it enables direct comparison to light microscopy. For example, the same thin section could be used to obtain statistically significant universal stage orientation data to estimate shock pressures. Using a TEM, the same type of measurements can only be made on a few grains. Therefore, reliable SEM methods to identify PDFs in quartz would form a welcome addition to TEM observations. Furthermore, SEM techniques are nondestructive, which is a great advantage in the study of shocked minerals.

Gratz et al. (1996) already showed that etching techniques and secondary electron (SE) imaging provide an unambiguous criterion for distinction of PDFs and tectonic deformation lamellae: amorphous PDFs etch out when treated with HF acid; tectonic deformation lamellae, in contrast, do not exhibit such well-developed etching patterns (Wegner and Christie 1983). Cathodoluminescence (CL) imaging, both in light microscopy and in an SEM, is a technique that has been used to image shocked quartz grains in general (Ramseyer et al. 1992; Trepmann et al. 2005) and PDFs in quartz in particular (Seyedolali et al. 1997; Boggs et al. 2001; Gucsik et al. 2003; Cavosie et al. 2010), but no comparison of PDFs with tectonic deformation lamellae has been made. Seyedolali et al. (1997) used CL to determine the provenance of quartz grains from different settings, including impact sites and stratigraphic impact layers. They found that PDFs can be imaged using a CL detector attached to an SEM, although Gucsik et al. (2003) did not report PDFs in SEM-CL images of experimentally shocked quartzites. Cavosie et al. (2010) imaged shocked quartz grains from the Vredefort crater, showing that basal (Brazil twin type) PDFs can also be observed with SEM-CL. Boggs et al. (2001) used SEM-CL methods to show that in CL images, PDFs can be distinguished from healed tectonic microfractures, but this is the only tectonic structure they looked at, and they did not consider tectonic
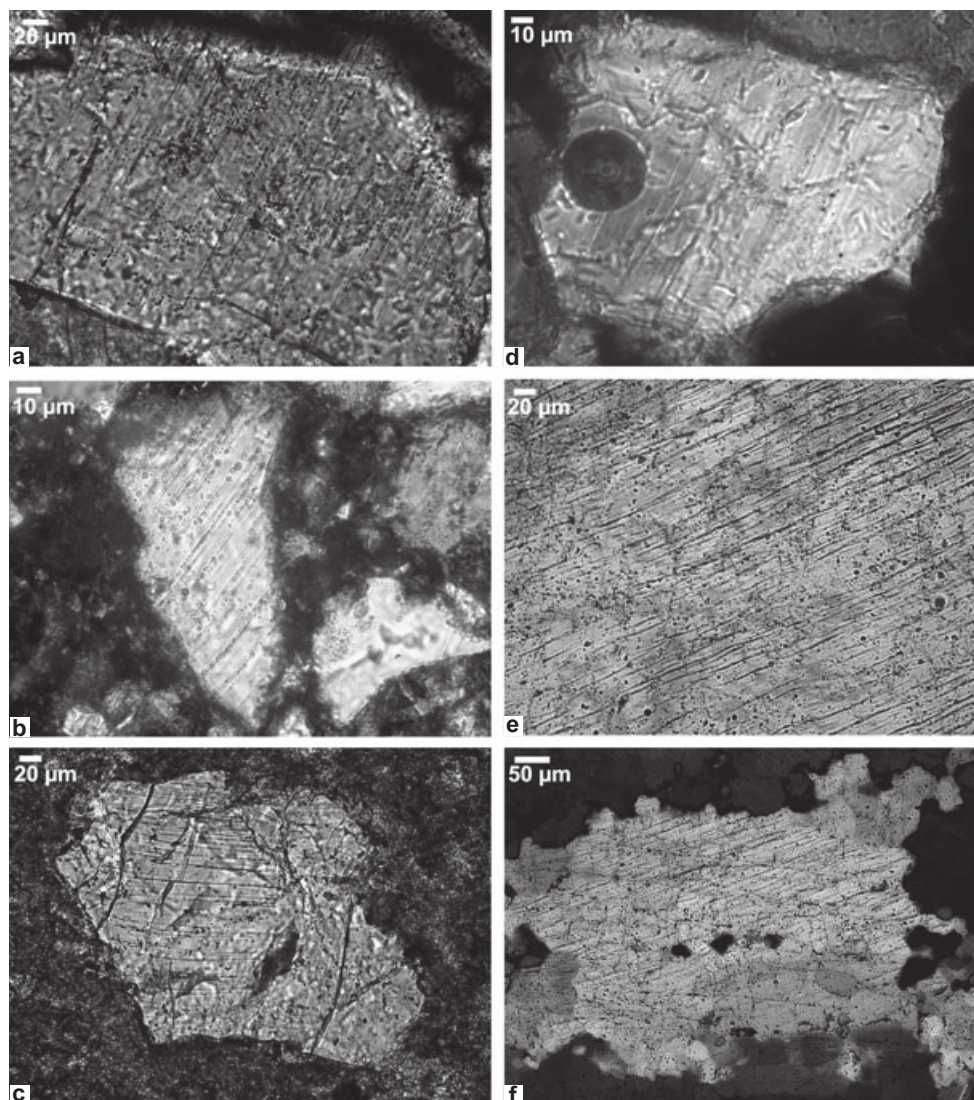
Fig. 1. Light microscopic images of PDFs in grains from Vredefort (a), Rochechouart (b and c), and of tectonic deformation lamellae from Flinders Ranges, Australia (d), and the Belgian Ardennes (e and f). Especially the PDFs from Vredefort (a) and tectonic deformation lamellae from Flinders Ranges (d) look similar on first inspection. Images a, b, c, and f are taken with cross-polarized light; images c and e with plane-polarized light.

deformation lamellae. We used SEM-CL imaging techniques, both grayscale (limited wavelength) and composite color, to study known examples of PDFs and of tectonic deformation lamellae in quartz to define characteristics that can be used to identify PDFs and distinguish them from other, nonshock-related lamellar microstructures. In this article, we primarily aim to provide an easy, low-cost method to reliably distinguish between PDFs and tectonic deformation lamellae and not to explain the CL behavior of the structures in detail, but some possible interpretations of the CL emission of PDFs will be discussed.

SAMPLES AND METHODS

Samples and Imaging Techniques

Two SEM systems, each equipped with a CL detector, were used to record CL images in this study. Both systems are located at the Electron Microscopy Laboratory at Utrecht University in the Netherlands. The first system is a Philips XL30S FEG SEM equipped with a Centaurus CL detector (K.E. Developments Ltd, Cambridge, UK), which has a wavelength detection range of 300–650 nm with a peak at 420 nm, and is
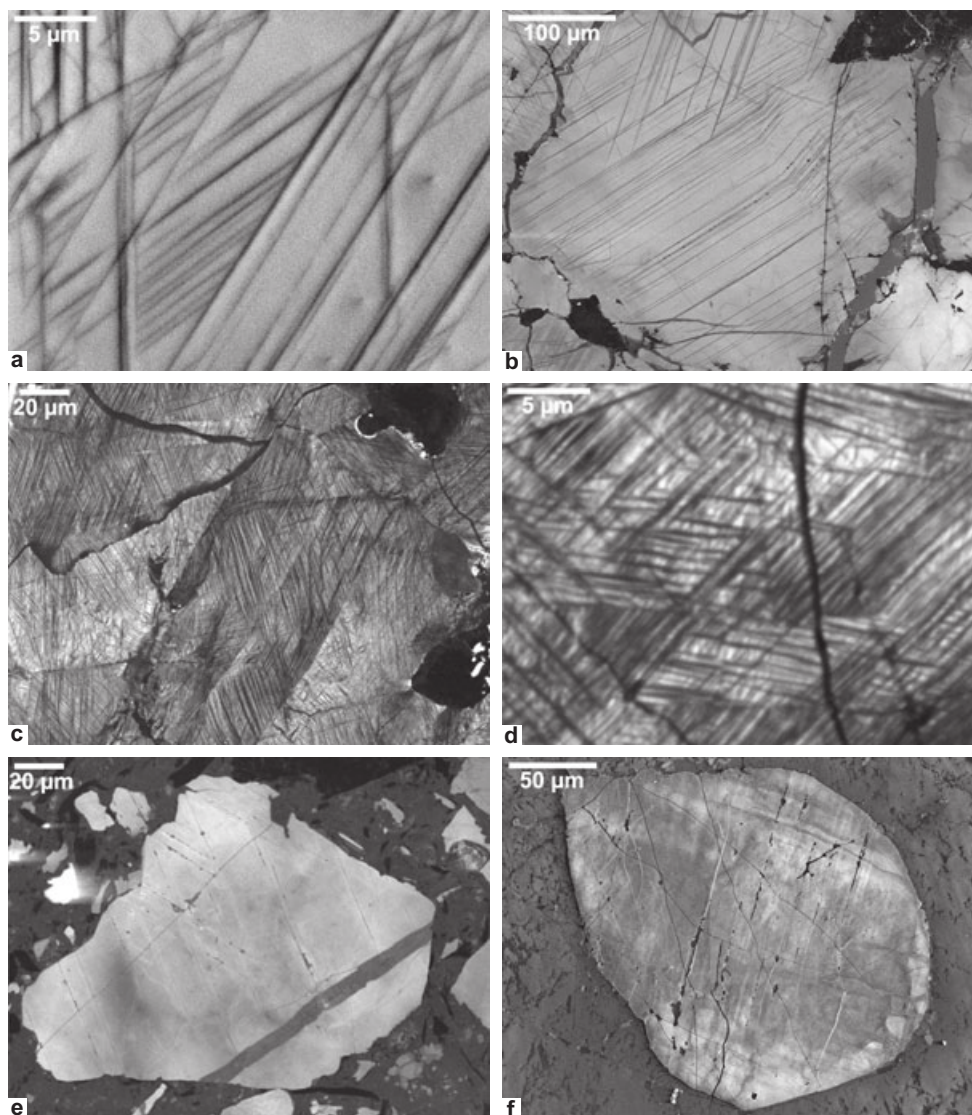
Fig. 2. Limited wavelength CL images of PDFs from the Ries (a-d), Rochechouart (e), and Vredefort (f) impact structures. PDFs are visible in the Ries and Rochechouart samples, but in the Vredefort sample, they can only be recognized from the traces of holes or fluid inclusions. The semi-linear features in the top of the Vredefort grain (f), running NE-SW, are not PDFs, and are not visible in the light microscope.

thus most sensitive to blue to violet light. In addition, the samples were studied in an FEI Nova Nanolab 600 SEM with Gatan PanaCL detector (Gatan UK, Oxford, UK). The PanaCL detector is more or less panchromatic, and has a detection range of 185–850 nm. Three color filters (red, green, and blue) can be fitted to the Gatan detector for recording color filtered images. The red filter primarily transmits light in the range 595–850 nm, the green filter in the range 495–575 nm, and the blue filter in the range 185–510 nm. Both unfiltered and filtered images were recorded; the filtered images were subsequently combined into composite RGB color images in Adobe Photoshop, by including them in the red, green, and blue channels of a new image file. As red, green, and blue channels were optimized individually to obtain the maximum amount of information from the image, color information in the images is nonquantitative. The instruments were operated at an acceleration voltage of 5–10 kV and with a beam current of 1.6–6.3 nA, at room temperature. For comparison, 10 shocked quartz grains were also imaged at cryogenic temperatures, between −140 °C and −170 °C, using a liquid nitrogen-cooled cryostage in the Nova Nanolab 600 SEM with color filtered CL. In addition to the CL images, SE and, for most grains, light microscopic images were recorded. All samples are standard polished thin sections, which were carbon coated to prevent charging.

Grayscale (limited wavelength) CL images were recorded using the Centaur CL detector for 57 shocked quartz grains in eight samples from well-known impact structures that have been extensively studied (Ries, Rochechouart, Popigai, and Vredefort), and for nine grains in one sample containing tectonic deformation lamellae from the Flinders Ranges, Australia. For color CL, using the Gatan PanaCL detector, 51 quartz grains containing PDFs were studied in 13 different samples from the same impact structures. Six grains from the Ries crater and four grains from the Popigai crater were also imaged at temperatures between −140 °C and −170 °C. Furthermore, 27 grains with tectonic deformation lamellae were studied in six samples from three locations (Flinders Ranges, Australia; the Belgian Ardennes; and Cantabria, Spain). These numbers are summarized in Table 1. In several cases, the same grains were studied with the two different SEM-CL systems for comparison.

Although the Flinders Ranges in the Adelaide Fold Belt, from which the Australian deformation lamellae samples were taken, is within the range of the ejecta layer of the Late Neoproterozoic Acraman impact structure (Williams and Gostin 2005), we are quite certain that the samples do not come from this impact layer. The samples were taken from massive quartzite layers such as the ABC quartzite, whereas the impact ejecta are found in the Bunyeroo mudstone formation.

Cathodoluminescence Background

When an electron beam hits a sample in an SEM, several types of beam-sample interaction can occur. One result is that electrons can be excited to a higher energy level. When excited electrons fall back to their original state, either directly or via a trap (in the form of a lattice defect, impurity, or vacancy), photons can be emitted with energies in the infrared, visible, or ultraviolet wavelength ranges. This photon emission is the basis of CL. The wavelength (and thus the color) and intensity of the emitted photons vary depending on the mineral composition of the sample (intrinsic luminescence) and on the number and nature of defects and impurities in the material (extrinsic luminescence). Quartz can exhibit several different CL colors, ranging from bright blue to red, brown, or nearly nonluminescent. Several studies have attempted to use CL color and intensity as a provenance tool (e.g., Zinkernagel 1978; Seyedolali et al. 1997; Boggs et al. 2002; Bernet and Bassett 2005), but there is too much overlap in the color ranges to make this a reliable quantitative method (Boggs et al. 2002). Furthermore, the crystallographic orientation of quartz grains can have a significant effect on CL color (Walderhaug and Rykkje 2000). In general, volcanic quartz has blue CL color, whereas plutonic, metamorphic,

and hydrothermal quartz CL colors range from blue to red (Marshall 1988; Boggs et al. 2002).

The CL emission of quartz depends on many factors such as the degree of ordering in the crystal lattice; vacant lattice sites; trace amounts of activators such as Fe^{3+}, Al^{3+}, H^+, Li^+, Na^+, K^+, and Ti^{4+}; water content; or damage resulting from radiation, strain, or shock (Marshall 1988; Ramseyer and Mullis 1990; Perny et al. 1992). Recently, many studies have focused on the causes of CL intensity differences in quartz (Rusk and Reed 2002; Landtwing and Pettke 2005; Rusk et al. 2006) and of specific emission bands in the CL spectra of quartz and other forms of SiO_2 (Ramseyer and Mullis 1990; Perny et al. 1992; Stevens Kalceff and Phillips 1995; Stevens Kalceff et al. 2000; Götze et al. 2001; Trukhin et al. 2003, 2004; Götze and Kempe 2008; Stevens Kalceff 2009). Common emission bands are around 340 nm (Al and Li impurities), 420 nm (intrinsic emission), and 620–650 nm (nonbridging oxygen hole center, NBOHC) (Stevens Kalceff and Phillips 1995; Stevens Kalceff et al. 2000; Götze et al. 2001), but many more are described in the literature. The relative intensities of the dominant emission bands in the visible light range (380–700 nm) determine the CL color that is perceived by the eye (Götze et al. 2001).

Shocked quartz is generally blue luminescent, with an additional emission band at 630–650 nm (Ramseyer et al. 1992; Ramseyer and Mullis 2000; Trepmann et al. 2005; Götte 2009; Okumura et al. 2009; Kayama et al. 2010), although the 630–650 nm band was not observed in experimentally shocked quartzite (Gucsik et al. 2003).

RESULTS

Grayscale Cathodoluminescence

In the limited wavelength grayscale SEM-CL images (Fig. 2), PDFs appear as well-defined, narrow darker lines that are nonluminescent in contrast to the host quartz grains, which are lighter in the CL images. Usually, the PDFs are straight and of constant thickness (Fig. 2a, b, and e), but in some grains, they appear slightly curved and show slight thickness variations (Fig. 2c and d). In all of these grains, multiple sets of PDFs are present (at least three, often four or more), and they are very closely and regularly spaced, thicker, and have slightly wavy edges. PDFs from different impact structures show the same CL characteristics; only in the Vredefort samples (Fig. 2f) no clear PDFs are visible in the grayscale images.

Tectonic deformation lamellae in grayscale SEM-CL images (Fig. 3) can either be more luminescent than the host quartz grain or nonluminescent. In general, the lamellae have slightly wavy features with a varying

Table 1. Sample locations and properties.

Sample	Location	Rock type	Lat/lon (WGS84)	Nr. of grains			PDF luminescence	Grain luminescence
				PanaCL	Centaurus	Cryo		
OTT-1	Ries (Germany), Otting	Suevite	48°52'32.07"N/10°47'42.37"E	1	3	–	Nonluminescent	Red
OTT-2	Ries (Germany), Otting	Suevite	48°52'32.07"N/10°47'42.37"E	3	16	6	Red/nonluminescent	Blue/red to blue
RI-37	Ries (Germany), Aumühle	Granite fragment (loose block, probably from suevite)	48°58'16.84"N/10°37'43.95"E	3	6	–	Red	Blue
RI-43	Ries (Germany), Polsingen	Gneiss fragment from impact melt rock	48°55'4.61"N/10°42'19.36"E	3	2	–	Nonluminescent	Red
RI-47	Ries (Germany), Polsingen	Granite fragment with quartz vein from impact melt rock	48°55'4.61"N/10°42'19.36"E	2	5	–	Nonluminescent/red	Red/blue
MRO-3	Rochechouart (France), Montoume	Impact melt rock	45°46'31.94"N/0°46'30.01"E	4	–	–	Red	Reddish brown or blue
MRO-4	Rochechouart (France), Montoume	Impact melt rock	45°46'31.94"N/0°46'30.01"E	3	–	–	Nonluminescent/red	Red/reddish brown or blue
MRO-5	Rochechouart (France), Montoume	Impact melt rock	45°46'31.94"N/0°46'30.01"E	9	–	–	Nonluminescent/red	Red/reddish brown or blue
RO-2	Rochechouart (France), Rochechouart	Lithic breccia		6	23	–	Red	Blue
P2	Popigai (Russia)	Impact melt rock	71°45'31.00"N/110°15'10.00"E	4	1	4	Nonluminescent/red	Red/blue
E3	Vredefort (South Africa)	Granulite (Inlandsee Leucogranofels)	26°58'15.24"S/27°23'18.96"E	3	1	–	Red	Blue
H4	Vredefort (South Africa)	Granulite (Inlandsee Leucogranofels)	26°58'15.24"S/27°23'18.96"E	6	–	–	Red	Blue
VTM12C	Vredefort (South Africa)	Granite gneiss	For location see Fig. 1 of Cloete et al. 1999 (same location as sample VTM1.1)	4	–	–	Red	Blue
SARB-03	Flinders Ranges (Australia), south of Wilpena Pound	ABC quartzite	31°39'14.81"S/138°35'15.11"E	2	9	–		Blue to purple with red rims/red

Table 1. *Continued.* Sample locations and properties.

| Sample	Location	Rock type	Lat/lon (WGS84)	Nr. of grains PanaCL	Centaurus	Cryo	PDF luminescence	Grain luminescence
SAPP-02	Flinders Ranges (Australia), south of Pichi Pichi Railway Bridge	Quartzite	32°26′7.29″S/137°58′37.41″E	5	–	–		Red
B14	High Ardennes Slate Belt (Belgium)	Quartz vein	49°47′54.92″N/5°13′11.16″E	3	–	–		Red
HV07A	High Ardennes Slate Belt (Belgium)	Quartz vein	49°47′54.92″N/5°13′11.16″E	3	–			Red
HV07B	High Ardennes Slate Belt (Belgium)	Quartz vein	49°47′54.92″N/5°13′11.16″E	4	–			Blue with red rims/red
CV4	Bayas Fault Zone, Cantabria (Spain) (Blenkinsop and Drury 1988; Drury 1993)	Quartzite						
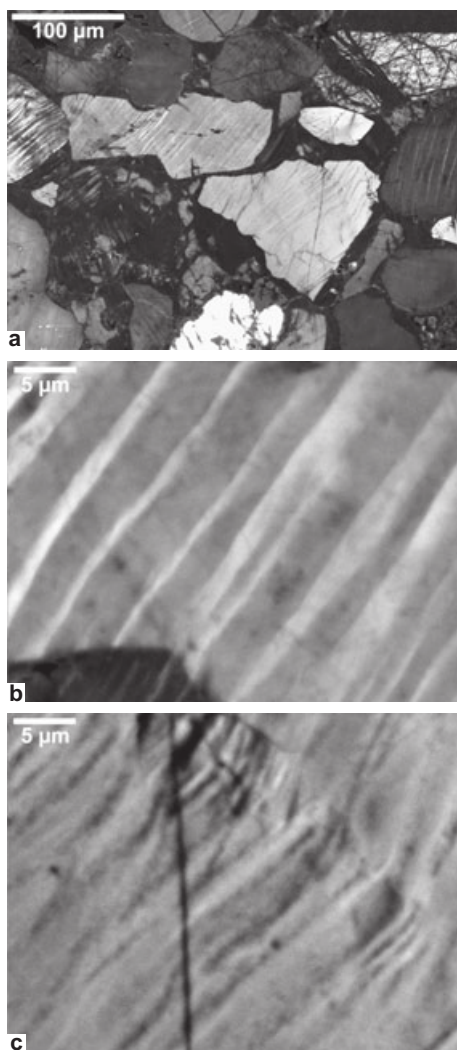
Fig. 3. a) Limited wavelength CL images of tectonic deformation lamellae from the Flinders Ranges. b) Close-up of the grain above and left of the center in a. c) Close-up of the grain below and right of the center in a.

thickness; they are thicker and much less well-defined than the PDFs in Fig. 2.

Composite Color Cathodoluminescence

In terms of shape and thickness, PDFs in the composite color SEM-CL images (Fig. 4) are identical to the limited wavelength images (Fig. 2). However, it is evident that the PDFs are usually luminescent and mainly emit red light (Fig. 4a–f, and i) which differs from the CL information in the grayscale images shown in Fig. 2. This is true for most PDFs, including the Vredefort samples (Fig. 4e and f), and in host quartz grains, which have different CL colors, ranging from red and brown to purple and blue. The red emission of the

PDFs becomes brighter with increasing scanning time and after repeated scanning with the electron beam, making them more easily discernable. Only in highly shocked grains with multiple sets of closely spaced PDFs are the lamellae nonluminescent (Fig. 4g and h). This is the case in the grains that show more, thicker, less straight, and more sets of PDFs in limited wavelength images. Fig. 4g also shows that partly red, partly nonluminescent PDFs occur (bottom right, SW-NE trending set). Red-luminescent PDFs usually occur in violet to blue-luminescent host quartz (Fig. 4a, b, e, f, and i), although also in Rochechouart grains, reddish-brown host quartz is observed (Fig. 4c and d). Nonluminescent PDFs most often occur in red-luminescent host quartz (Fig. 4h), but in some cases, the host quartz shows both red and blue luminescent parts (Fig. 4g).

Composite color images of tectonic deformation lamellae (Fig. 5) are very similar to the limited wavelength images shown in Fig. 4, but differ very much from the color images of PDFs. Although shape and thickness alone are clearly sufficient to distinguish between tectonic deformation lamellae and PDFs, the CL color information further emphasizes the different appearance of the two microstructures. While PDFs are consistently red or nonluminescent, tectonic deformation lamellae show a range of colors from blue to red. It is not always clear where host quartz and tectonic lamella begin or end, or even which part of the grain should be defined as "grain" or "lamella." Due to their variable CL emission and the vague boundaries between lamellae and host quartz, in both grayscale and color CL images, it is very difficult to accurately define and measure the spacing and thickness of tectonic deformation lamellae. PDFs on the other hand have sharp boundaries, and a clear distinction can be made between PDF and host quartz, making accurate measurements of their (apparent) spacing and thickness possible.

Table 2 summarizes the characteristics of both PDFs and tectonic deformation lamellae in CL images.

Secondary Electron Imaging

Secondary electron images of two tectonically deformed and six shocked quartz grains are shown in Fig. 6. Tectonic deformation lamellae (Fig. 6a and 6b) are barely detectable in SE images. In some grains, they show up as more or less linear, but relatively broad (compared with decorated PDFs), traces of fluid inclusions (Fig. 6b, through the center from top left to bottom right). PDFs are only visible in SE images when they are decorated; these PDFs show up as strictly linear traces of tiny holes or fluid inclusions (Fig. 6d). It is clear from Fig. 6c that undecorated PDFs cannot be
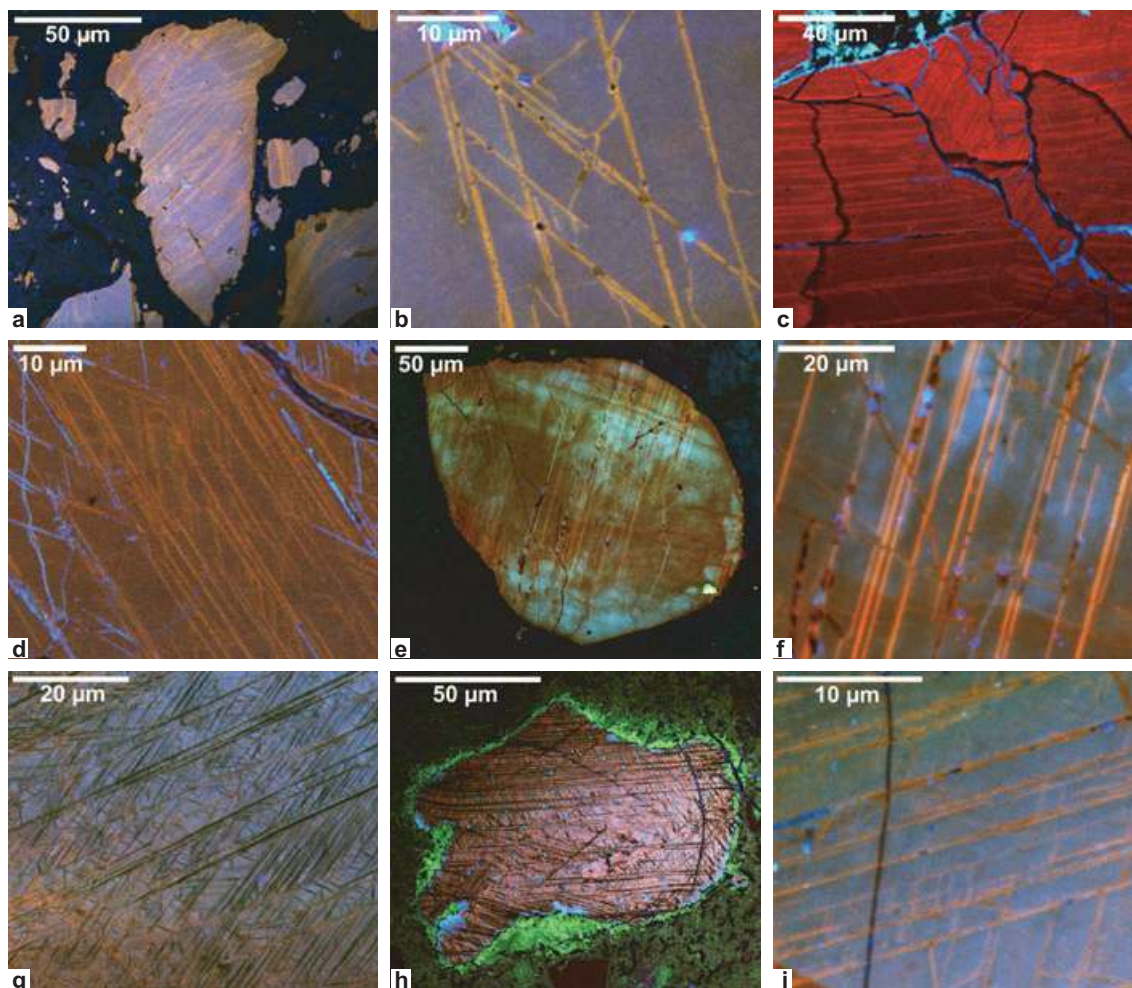
Fig. 4. Composite color CL images of PDFs from a) Rochechouart—same grain as in Fig. 1b. b) Rochechouart—higher magnification image of the grain in Fig. 2e. c) Rochechouart—higher magnification image of the grain in Fig. 1c. d) Rochechouart. e) Vredefort—same grain as in Fig. 2f. f) Vredefort—higher magnification of the grain in Fig. 4e and 2f. g) Ries. h) Popigai. i) Popigai. In all samples, including those from Vredefort, PDFs are clearly visible as either red or nonluminescent linear features. Bright blue-luminescent spots are caused by remains of aluminum oxide polishing grains.

recognized in SE images (compare Fig. 6c to Fig. 4d, where the same grain shows multiple sets of PDFs in the color CL image that are invisible in the SE image). In some grains where many sets of closely spaced PDFs are present, the PDFs are not decorated by small holes, but are partly open features (as in Fig. 6e). It seems that these partly open PDFs are always of the nonluminescent type, whereas both "normal" decorated and undecorated PDFs are red luminescent (in between the fluid inclusions, in the case of decorated PDFs). The nonluminescence occurs not only in the open parts of these PDFs, where there is no material to produce a CL signal but also in the rest of the lamellae (compare Fig. 4g and 6e). Therefore, there is a genuine lack of CL signal in these PDFs.

Cryogenic Composite Color Cathodoluminescence

Figure 7 shows composite color images of the same grains, recorded at room temperature and at −140 °C or −170 °C. Using the liquid nitrogen-cooled cryostage, the intensity of the CL emission strongly increases, especially in the blue and green color ranges. In most cases, the overall color characteristics of the shocked quartz grains remain the same: red-luminescent and nonluminescent PDFs occur, although the CL color of the host quartz often changes slightly at cryogenic temperature. However, in some grains that contain the nonluminescent type of PDFs at room temperature, red-luminescent PDFs appear at cryogenic temperatures that are not visible at room temperature (compare Fig. 4h with Fig. 7f and 7i).

For many grains, the image quality is better at room temperature than at cryogenic temperatures. As a result of the extreme increase in intensity of the blue emission, there is less detail in the cryo-CL images (compare Fig. 7g and h, or Fig 4h and 7f).

DISCUSSION

Distinction Between Planar Deformation Features and Tectonic Deformation Lamellae

The most important characteristics of PDFs and deformation lamellae are summarized in Tables 1 and 2. Our results show that CL imaging is a very promising method to distinguish between shock and tectonic deformation lamellae, even on a visual basis alone. In cases where only one or two sets of lamellar microstructures are present, which could lead to misidentification in a light microscope, the CL characteristics of the structures clearly show whether they are PDFs or tectonic deformation lamellae (Figs. 2–5): PDFs are thin, straight lines that are dark in grayscale CL images, and red or nonluminescent in composite color CL images, whereas tectonic deformation lamellae are less well defined, thicker, and slightly wavy, with varying thickness, and can show varying CL colors in composite color images.

The physical basis of the difference in CL emission between shocked and tectonically deformed grains remains unclear, and requires further research into the relationship between the CL emission and the nature of the different microstructures. However, even without knowing the exact cause of the CL signal, SEM-CL imaging appears to be a useful technique to distinguish between tectonic and shock lamellae, and to identify PDFs in quartz.

Spacing and (apparent) thickness of planar microstructures in quartz have been mentioned as characteristic features to distinguish between tectonic and shock lamellae (Stöffler and Langenhorst 1994; Grieve et al. 1996; French and Koeberl 2010), but are in practice not often used quantitatively. In general, tectonic deformation lamellae are thicker, more widely spaced, and usually slightly curved, whereas PDFs are extremely thin, closely spaced, and straight (Alexopoulos et al. 1988; Lyons et al. 1993). However, these are not definitive criteria; a range of different types of tectonic deformation lamellae has been recognized (Christie and Raleigh 1959; White 1973; Christie and Ardell 1974; Drury 1993; Vernooij and Langenhorst 2005). For both PDFs and tectonic deformation lamellae, there are many cases in which spacing, thickness, and straightness deviate from the "standard" values. Even in a relatively small sample set such as ours, these characteristics show considerable variation, which is obvious from Fig. 2 to 5.

Whereas the PDF spacing depends on the impact pressure, the spacing of tectonic deformation lamellae depends on stress level (Koch and Christie 1981). Tectonic lamellae may occur that are as closely spaced as PDFs (see for example the tectonic lamellae in Fig. 5d, e, and f). Furthermore, spacing and thickness measurements will depend on the imaging method used; in SEM-CL images, for example, more and thinner individual lamellae can be recognized than in light microscopic images, and thus the results of spacing and thickness measurements could differ if the size and spacing of the PDFs are below the spatial resolution for the imaging method used. The spatial resolution of a standard light microscope is theoretically limited to approximately 200–400 nm (Nesse 2004), but is worse in practice. It is known from TEM measurements that many PDFs and some types of tectonic deformation lamellae are thinner than this limit (McLaren et al. 1970; Langenhorst 1994; Stöffler and Langenhorst 1994), and some of these lamellae, therefore, will not be detected in a light microscope. As already mentioned in the section Composite Color Cathodoluminescence, it is questionable whether it is at all possible to perform reliable measurements of spacing and thickness on tectonic deformation lamellae. Tectonic deformation lamellae are not as clearly defined as PDFs. In CL images, it is not always evident which part of the grain is lamella and which part is host quartz (see for example Fig. 3c, 5b, 5c, and 5e). McLaren et al. (1970) also pointed out that in a light microscope, tectonic deformation lamellae are most easily observed when the microscope is focused on the upper surface of the thin section, and that when the lamellae are exactly in focus (which would be required for accurate thickness measurements), they are almost invisible. Thus, measurements on tectonic deformation lamellae are difficult and unreliable.

The presence of multiple, differently oriented sets of (indexed) planar features in a quartz grain of course remains a good indicator for shock, but in cases where light microscopy shows only one or two sets of lamellae, and when it is not immediately obvious whether these are shock or tectonic lamellae, CL imaging can distinguish between the two. In addition to the shape criteria described above, CL images often show more sets of PDFs than can be observed in light microscopy. This is readily seen when comparing, for example Fig. 1c and Fig. 4c, or Fig. 1b and Fig. 4a, which show the same grain in a light microscopic and color CL image, respectively.

Filtered, color, and cryo-CL imaging and CL spectroscopy can all provide extra information on the nature of planar microstructures in quartz. However, unfiltered grayscale CL images will, in many cases, be sufficient to distinguish PDFs from tectonic deformation lamellae and show features that are unclear in light microscopy.
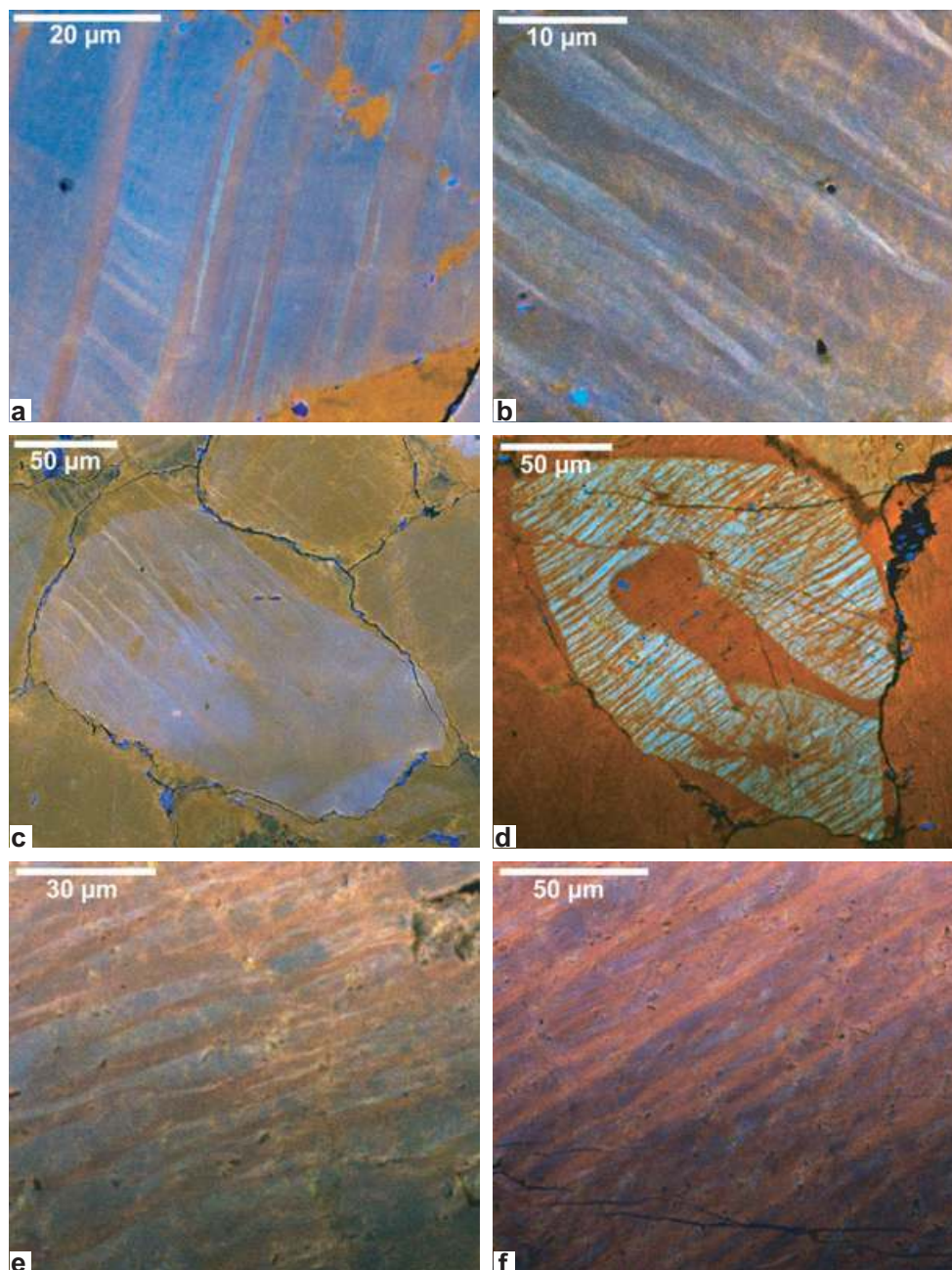
Fig. 5. Composite color CL images of tectonic deformation lamellae from Flinders Ranges (a—same grain as in Fig. 1d; b and c), Cantabria (d), and the Ardennes (e and f). Bright blue-luminescent spots are caused by remains of aluminum oxide polishing grains.

All our shocked samples are from impact structures in predominantly crystalline, nonporous target rocks. As a result of the porosity of sedimentary target rocks, the shock wave energy is distributed much more heterogeneously than in crystalline targets. As a result, shock effects representative of different shock stages in the classification for nonporous rock types can occur together in porous rocks (Grieve et al. 1996). However, the same types of shock effects occur, and there is essentially no structural difference between PDFs in quartz grains from crystalline (nonporous) or from sedimentary (porous) target rocks (Kieffer 1971; Kieffer et al. 1976). We therefore do not expect that the CL characteristics from PDFs in quartz from sedimentary rocks differ so much from those in crystalline rocks, and that the distinction between PDFs and tectonic

Table 2. Cathodoluminescence characteristics for planar deformation features and tectonic deformation lamellae.

	Planar deformation features	Tectonic deformation lamellae
CL color	Red/non	Red/blue
Number of sets	(Usually) multiple	Usually one, rarely two
"Sharpness"	Very well defined	Hard to distinguish lamellae from host quartz
Thickness	(Usually) thin	(Usually) much thicker
Spacing	Variable, but usually closely spaced	Closely spaced
Straightness	Straight	Slightly curved, subplanar

deformation lamellae becomes impossible. Future research is needed to show how the extra heat production involved in impacts into porous rocks might affect the CL emission of (parts of) shocked quartz grains.

Cathodoluminescence Characteristics of Planar Deformation Features in Quartz

Cryo-Cathodoluminescence

In contrast to many other minerals, such as feldspars, calcite, or zircons, quartz does not exhibit high intensity CL emission at room temperature. At temperatures below −80 to −100 °C, the CL emission of quartz shows a dramatic increase in intensity by factors of 100–1000 (Marshall 1988) so to get the highest intensity signal, CL work is often carried out at low temperature. In our low temperature comparison, the intensity of the CL emission strongly increased, as expected, especially in the blue and green range. However, the overall results at cryogenic temperatures were the same as those found at room temperature: both red- and nonluminescent PDFs are present, and in most cases also the CL color of the host quartz does not change significantly. These results show that, although cryo-CL does give a higher intensity CL emission, cryo is not required to image shocked quartz grains and identify PDFs. On the contrary, as Boggs et al. (2001) already observed, the quality of the CL images is often better at room temperature than at cryogenic temperatures. Although cryo-CL can often provide extra information, even the simplest method of SEM-CL imaging, at room temperature, produces high quality images that are sufficient to identify PDFs in quartz and distinguish them from tectonic deformation lamellae.

Cathodoluminescence of Shocked Quartz

Boggs et al. (2001) reported that PDFs can be imaged with SEM-CL methods, and concluded that PDFs are visible in CL images because they are nonluminescent in contrast to the host quartz grain. Our results show that the latter is not the case; in fact, most PDFs do emit light, mostly in the red to infrared wavelength range (595–850 nm, red filter). PDFs often appear nonluminescent in (panchromatic) CL images, because the intensity of the (usually) blue light emitted

by the surrounding quartz is often so much higher than the intensity of the signal coming from the material in the PDFs. In the case of Boggs et al. (2001), the apparent nonluminescence of the PDFs might also be a result of the CL detector they use, which has a detection range of about 185–700 nm, and detects (part of) the ultraviolet and the complete blue wavelength range, but does not detect all of the red range (620–750 nm), and none of the infrared wavelengths. The PDFs could appear nonluminescent because of the low intensity of the CL signal emitted by the PDFs and the limited range of the detector, although this would depend on the specific wavelength of the CL emission of the PDFs. In the images recorded with our blue-sensitive limited wavelength CL detector, PDFs are dark because they emit red light, which is not detected, and therefore the structures appear to be nonluminescent. Several studies have shown that shocked quartz is usually blue luminescent, with an additional emission band at 630–650 nm (Ramseyer et al. 1992; Ramseyer and Mullis 2000; Trepmann et al. 2005; Götte 2009; Okumura et al. 2009; Kayama et al. 2010). The red-luminescent PDFs observed in our samples could (partly) be the source of this band.

The two types of CL behavior observed in PDFs (red to infrared or nonluminescent) are possibly related to shock intensity. Nonluminescence of PDFs only occurs in grains with multiple sets of closely and regularly spaced, thicker PDFs (Fig. 4g and h), which indicate high shock pressure (Grieve et al. 1996; Ferrière et al. 2008). Okumura et al. (2009) found that shocked quartz grains from the Ries crater show the usual emission bands with maxima around 385 nm (violet) and around 650 nm (red). The 650 nm band is observed independent of shock pressure, whereas the 385 nm band dissapears in more highly shocked grains. This seems to be in line with the observation that nonluminescent PDFs usually occur in highly shocked, red-luminescent quartz grains. Red CL emission of PDFs is seen in grains with a lower number of sets of PDFs, which are more widely and less regularly spaced and are therefore interpreted as the result of lower shock pressure.

Most of the PDFs from the Vredefort impact structure occur in single sets and are of the basal, Brazil
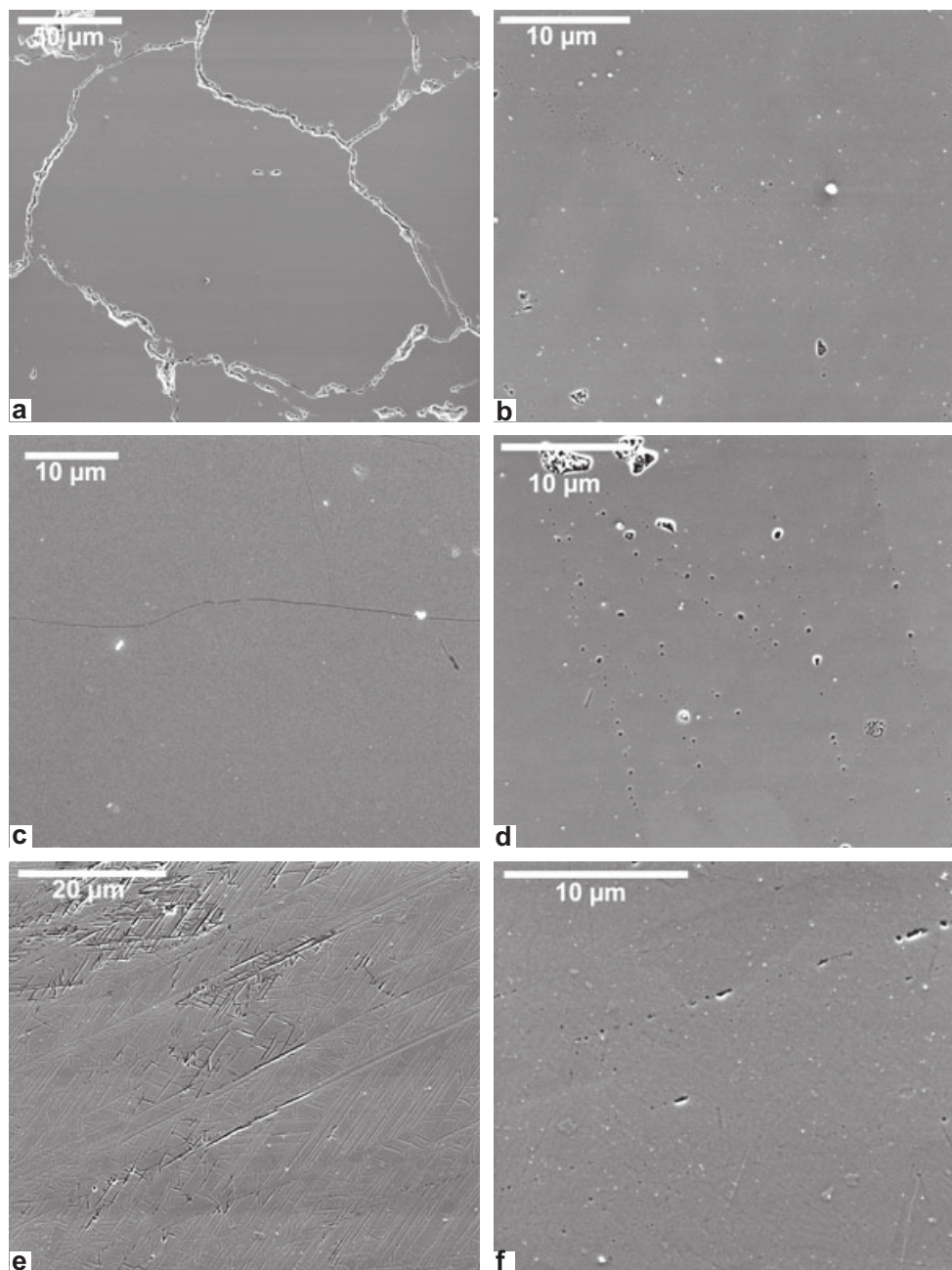
Fig. 6. Secondary electron images of a) Tectonic deformation lamellae from Flinders Ranges—same grain as in Fig. 5c. b) Tectonic deformation lamellae from Flinders Ranges—same grain as in Fig. 5b. c) Undecorated PDFs from Rochechouart—same grain as in Fig. 1c and 4c. Note that the PDFs in this grain can be seen in both light microscopic and CL images, but are invisible in this SE image. d) Decorated PDFs from Rochechouart—same grain as in Fig. 2e and 4b. e) PDFs from Ries—same grain as Fig. 4f. Black linear features in this image are open PDFs; other contrast is probably the result of some slight orientation contrast detected. f) PDFs from Popigai—same grain as in Fig. 4g. Some PDFs are decorated, but most are not (note that they can be recognized in the CL image in Fig. 4g).

twin type (Carter 1965; Grieve et al. 1990; Leroux et al. 1994). In our Vredefort samples, we observed only grains with one set of PDFs so it is likely that most of these are basal PDFs. It is striking that the characteristic red CL emission is observed in features that have a fundamentally different structure: in PDFs that are considered amorphous (Ries) as well as in basal, Brazil twin type PDFs (Vredefort) and decorated PDFs (Rochechouart, Popigai). An explanation for this is not apparent from the CL images alone and will require further research into the
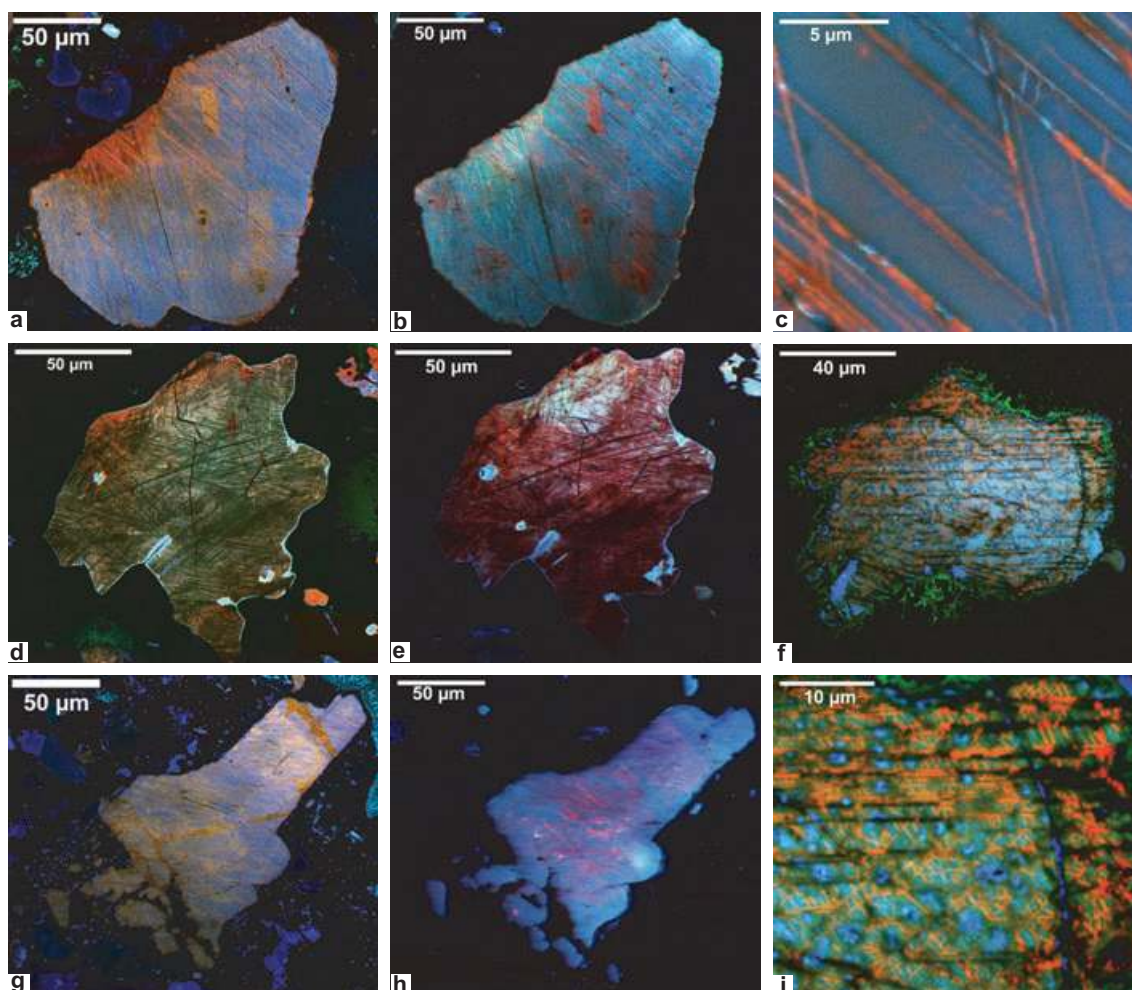
Fig. 7. Composite color CL images recorded at room temperature (RT) and at cryogenic temperatures. a) Shocked quartz grain from the Ries crater, showing red-luminescent PDFs, RT. Red patches are beam damage from earlier scanning. Same grain as in Fig. 2a. b) Same grain as in a, −140 °C. c) Higher magnification of the grain in a and b, −140 °C. Small irregularities in the PDFs are a relict of slight charging of the sample. d) Shocked quartz grain from the Ries crater, showing nonluminescent PDFs, RT. e) Same grain as in d, −170 °C. f) Shocked quartz grain from the Popigai crater, same grain as in Fig. 4h, −170 °C. At RT, this grain contains nonluminescent PDFs, and the host quartz is red luminescent. At −170 °C also, red-luminescent PDFs appear and the host quartz shows more blue CL. g) Shocked quartz grain from the Ries crater, showing red-luminescent PDFs, RT. h) Same grain as in g, −170 °C. i) Higher magnification image of the grain in f, −170 °C. Bright blue spots in these images are remains of polishing grains.

exact nature of the defects, composition, or water content variations that might cause the typical red CL signal of PDFs.

Possible Causes of the CL Behavior of Planar Deformation Features and Difference between Red- and Nonluminescent PDFs

Several causes of red CL emission in quartz are mentioned in the literature. High water content or low Ti/Fe ratio can result in a red CL emission (Marshall 1988). Substitutional incorporation of Fe^{3+} into the quartz lattice probably gives rise to an emission band around 705 nm (red to infrared) (Götze et al. 2001). Fitting et al. (2001) observed a red peak (around 650 nm) in the CL spectrum of SiO_2 glass, indicating that also amorphous SiO_2 is capable of producing red CL (although, of course, CL color cannot prove anything on crystal structure). The most important red CL peak is the common 620–650 nm emission band in quartz. It consists of two overlapping components at 620 nm and at 650 nm, and can be caused by an oxygen vacancy or a nonbridging oxygen hole center (NBOHC, ≡Si-O, a dangling oxygen bond) (Stevens Kalceff and Phillips 1995; Stevens Kalceff et al. 2000; Götze et al.

2001). Different precursors for the NBOHC have been proposed that influence the band position. Among these precursors are hydrogen and sodium impurities, hydroxyl groups ($\equiv$Si-OH) (620 nm), peroxy linkages ($\equiv$Si-O-O-Si$\equiv$) (650 nm), and strained silicon-oxygen bonds (Si–O) (650 nm) (Stevens Kalceff and Phillips 1995; Götze et al. 2001).

The 650 nm emission increases during electron bombardment (Götze et al. 2001), which is an indication that this might be the emission of the red-luminescent PDFs, as they become brighter after repeated scanning with the electron beam. Furthermore, this emission band is commonly observed in shocked quartz grains (Ramseyer et al. 1992; Ramseyer and Mullis 2000; Trepmann et al. 2005; Götte 2009; Okumura et al. 2009; Kayama et al. 2010). Götte (2009) attributed the presence of a 630–650 nm emission band in shocked quartz from the Siljan and Araguainha craters to thermal breaking of OH groups, which are incorporated in the quartz. However, according to Stevens Kalceff et al. (2000), the emission related to the NBOHC with OH precursor is at 620 nm, and attenuates quickly under electron irradiation at room temperature. This does not fit our observation that the intensity of the emission in red-luminescent PDFs increases after repeated scanning.

Also, high water content or hydrogen impurities in the PDFs could explain the red luminescence, because H_2O is much more soluble in the amorphous material within PDFs than in the adjacent crystalline quartz (Grieve et al. 1996). The occurrence of basal PDFs decorated with tiny fluid inclusions illustrates that along Brazil twin boundaries, water content might also be locally increased, giving rise to the same CL behavior for the two different types of PDF.

A final explanation for the red luminescence of PDFs might be strained silicon-oxygen bonds. It is possible that strained Si-O bonds are present in the SiO_2 within PDFs (or were present before annealing), where the crystal structure is disordered or (partly) destroyed by the shock wave. These strained bonds could form the precursors for NBOHCs. Also, basal, Brazil twin PDFs might contain strained silicon-oxygen bonds as a result of the high differential stresses that form these structures during the shock event. Although no bonds need to be broken to form this type of twin, there will be some strain at the twin boundary (McLaren et al. 1970).

Of course, the above interpretations remain rather speculative and measurements of CL spectra of the emission from the PDFs could provide valuable extra information for the interpretation of the PDF characteristics in CL images.

The difference in CL emission between the red- and nonluminescent PDFs could be caused by structural differences of the material within the PDFs, as a result of increasing shock pressure and temperature. As mentioned previously, the occurrence of multiple sets of nonluminescent PDFs per grain, their close and regular spacing, and thickness and slightly wavy boundaries, all indicate formation under high shock pressures (Langenhorst 1994; Ferrière et al. 2008). According to the model presented by Langenhorst (1994), the transformation of crystalline quartz to diaplectic quartz glass is a process in which the number of dense, amorphous PDFs increases with increasing shock pressure and temperature, until the whole grain consists of diaplectic glass, with fluidal glass (lechatelierite) only occurring when the residual (postshock) temperature is sufficiently high. Three phases occur during this process: (1) when both shock and postshock temperatures are below the melting point of quartz, extremely narrow, straight PDFs, consisting of a superheated, dense, amorphous phase, form by solid-state transformation, to compensate for crystal lattice incompatibilities at the shock wave propagation front; (2) at higher shock pressure, the shock temperature increases to just above the quartz melting temperature, and the PDFs are at a sufficiently high temperature to melt a small region of the adjacent crystalline quartz, resulting in thicker PDFs with more wavy boundaries; and (3) when, at even higher shock pressure, the shock temperature is significantly higher than the quartz melting temperature, the crystalline regions between the PDFs melt completely and the whole grain transforms into diaplectic quartz, which is quenched before complete decompression.

In this model, the red-luminescent (rhombohedral) PDFs could form during the first stage, when no melt is formed, but an amorphous phase in which the quartz lattice is disordered, but retains some of its structure. The CL emission centers that form during this stage must either survive postshock annealing, or be a secondary feature, because the red-luminescent PDFs are also observed in altered impact structures, such as the Rochechouart structure. During the second stage, the thicker, nonluminescent PDFs form, filled with quartz melt or diaplectic glass, because of the higher temperature associated with higher shock pressure. The complete destruction of the quartz crystal structure might result in nonluminescence of the material within the PDFs.

CONCLUSIONS

Both grayscale (limited wavelength) and composite color SEM-CL images provide strong criteria for distinction between planar deformation features and tectonic deformation lamellae in quartz, based on shape, thickness variability, and straightness, with different CL color signatures when color CL images are recorded.

Color imaging is the most reliable technique, as it shows that PDFs occur as two main types: either red- or nonluminescent, whereas tectonic deformation lamellae show varying CL colors, ranging from blue to red. When color CL facilities are unavailable, grayscale CL images are, depending on the detection range of the CL detector, in most cases sufficient to distinguish shock from tectonic lamellae. Although the causes of the CL behavior of PDFs remain uncertain, SEM-CL imaging provides a promising qualitative method to identify PDFs in quartz and to distinguish them from tectonic deformation lamellae.

Editorial Handling—Dr. Gordon Osinski

REFERENCES

Alexopoulos J. S., Grieve R. A. F., and Robertson P. B. 1988. Microscopic lamellar deformation features in quartz: Discriminative characteristics of shock-generated varieties. *Geology* 16:796–799.

Becker L., Poreda R. J., Basu A. R., Pope K. O., Harrison T. M., Nicholson C., and Iasky R. 2004. Bedout: A possible end-Permian impact crater offshore of Northwestern Australia. *Science* 304:1469–1476.

Bernet M. and Bassett K. 2005. Provenance analysis by single-quartz-grain SEM-CL/optical microscopy. *Journal of Sedimentary Research* 75:492–500.

Blenkinsop T. G. and Drury M. R. D. 1988. Stress estimates and fault history from quartz microstructures. *Journal of Structural Geology* 10:673–684.

Boggs S., Krinsley D. H., Goles G. G., Seyedolali A., and Dypvik H. 2001. Identification of shocked quartz by scanning cathodoluminescence imaging. *Meteoritics & Planetary Science* 36:783–791.

Boggs S. Jr, Kwon Y.-I., Goles G. G., Rusk B. G., Krinsley D., and Seyedolali A. 2002. Is quartz cathodoluminescence color a reliable provenance tool? A quantitative examination. *Journal of Sedimentary Research* 72:408–415.

Böhm A. 1883. Ueber die Gesteine des Wechsels. *Zeitschrift für Kristallographie, Mineralogie und Petrographie* 5:197–214.

Carter N. L. 1965. Basal quartz deformation lamellae; a criterion for recognition of impactites. *American Journal of Science* 263:786–806.

Cavosie A. J., Quintero R. R., Radovan H. A., and Desmond E. M. 2010. A record of ancient cataclysm in modern sand: Shock microstructures in detrital minerals from the Vaal River, Vredefort Dome, South Africa. *Geological Society of America Bulletin* 122:1968–1980.

Christie J. M. and Ardell A. J. 1974. Substructures of deformation lamellae in quartz. *Geology* 2:405–408.

Christie J. M. and Raleigh C. B. 1959. The origin of deformation lamellae in quartz. *American Journal of Science* 257:385–407.

Cloete M., Hart R. J., Schmid H. K., Drury M., Demanet C. M., and Sankar K. V. 1999. Characterization of magnetite particles in shocked quartz by means of electron- and magnetic force microscopy: Vredefort, South Africa. *Contributions to Mineralogy and Petrology* 137:232–245.

Cordier P. and Gratz A. J. 1995. TEM study of shock metamorphism in quartz from the Sedan nuclear test site. *Earth and Planetary Science Letters* 129:163–170.

Cordier P., Vrána S., and Doukhan J. C. 1994. Shock metamorphism in quartz at Sevetin and Susice (Bohemia)? A TEM investigation. *Meteoritics* 29:98–99.

Drury M. R. 1993. Deformation lamellae in metals and minerals. In *Defects and processes in the solid state: Geoscience applications*, edited by Boland J. N. and Fitz Gerald J. D. Amsterdam: Elsevier Science Publishers B. V. pp. 195–212.

Engelhardt W. V. and Bertsch W. 1969. Shock induced planar deformation structures in quartz from the Ries crater, Germany. *Contributions to Mineralogy and Petrology* 20:203–234.

Ernstson K. and Fiebag J. 1992. The Azuara impact structure (Spain)—New insights from geophysical and geological investigations. *Geologische Rundschau* 81:403–427.

Ferrière L., Koeberl C., Ivanov B. A., and Reimold W. U. 2008. Shock metamorphism of Bosumtwi Impact Crater rocks, shock attenuation, and uplift formation. *Science* 322:1678–1681.

Ferrière L., Koeberl C., and Reimold W. U. 2009. Characterisation of ballen quartz and cristobalite in impact breccias: New observations and constraints on ballen formation. *European Journal of Mineralogy* 21:203–217.

Ferrière L., Koeberl C., Libowitzky E., Reimold W. U., Greshake A., and Brandstätter F. 2010. Ballen quartz and cristobalite in impactites: New investigations. *Geological Society of America Special Papers* 465:609–618.

Fitting H.-J., Barfels T., Trukhin A. N., and Schmidt B. 2001. Cathodoluminescence of crystalline and amorphous SiO_2 and GeO_2. *Journal of Non-Crystalline Solids* 279:51–59.

French B. M. and Koeberl C. 2010. The convincing identification of terrestrial meteorite impact structures: What works, what doesn't, and why. *Earth Science Reviews* 98:123–170.

French B. M., Cordua W. S., and Plescia J. B. 2004. The Rock Elm meteorite impact structure, Wisconsin: Geology and shock-metamorphic effects in quartz. *Geological Society of America Bulletin* 116:200–218.

Glikson A. 2004. Comment on "Bedout: A possible end-permian impact crater offshore of Northwestern Australia." *Science* 306:613b.

Goltrant O., Leroux H., Doukhan J.-C., and Cordier P. 1992. Formation mechanisms of planar deformation features in naturally shocked quartz. *Physics of The Earth and Planetary Interiors* 74:219–240.

Götte T. 2009. Petrological modifications in continental target rocks from terrestrial impact structures: Evidence from

cathodoluminescence. In *Cathodoluminescence and its application in the planetary sciences*, edited by Gucsik A. Berlin: Springer. pp. 45–60.

Götze J. and Kempe U. 2008. A comparison of optical microscope- and scanning electron microscope-based cathodoluminescence (CL) imaging and spectroscopy applied to geosciences. *Mineralogical Magazine* 72:909–924.

Götze J., Plötze M., and Habermann D. 2001. Origin, spectral characteristics and practical applications of the cathodoluminescence (CL) of quartz—A review. *Mineralogy and Petrology* 71:225–250.

Gratz A. J., Nellis W. J., Christie J. M., Brocious W., Swegle J., and Cordier P. 1992. Shock metamorphism of quartz with initial temperatures −170 to + 1000 °C. *Physics and Chemistry of Minerals* 19:267–288.

Gratz A. J., Fisler D. K., and Bohor B. F. 1996. Distinguishing shocked from tectonically deformed quartz by the use of the SEM and chemical etching. *Earth and Planetary Science Letters* 142:513–521.

Grieve R. A. F., Coderre J. M., Robertson P. B., and Alexopoulos J. 1990. Microscopic planar deformation features in quartz of the Vredefort structure: Anomalous but still suggestive of an impact origin. *Tectonophysics* 171:185–200.

Grieve R. A. F., Langenhorst F., and Stöffler D. 1996. Shock metamorphism of quartz in nature and experiment: II. Significance in geoscience (abstract). *Meteoritics & Planetary Science* 31:6–35.

Gucsik A., Koeberl C., Brandstatter F., Libowitzky E., and Reimold W. U. 2003. Scanning electron microscopy, cathodoluminescence, and Raman spectroscopy of experimentally shock-metamorphosed quartzite (abstract). *Meteoritics & Planetary Science* 38:1187–1197.

Kayama M., Nishido H., Endo Y., Sekine T., Gucsik A., and Ninagawa K. 2010. Estimation of shock pressure on quartz and alkali feldspar from Ries crater using cathodoluminescence spectroscopy (abstract #5192). 73rd Annual Meeting of the Meteoritical Society: New York, USA. *Meteoritics & Planetary Science* 45.

Kieffer S. W. 1971. Shock metamorphism of the Coconino Sandstone at Meteor Crater, Arizona. *Journal of Geophysical Research* 76:5449–5473.

Kieffer S. W., Phakey P. P., and Christie J. M. 1976. Shock processes in porous quartzite: Transmission electron microscope observations and theory. *Contributions to Mineralogy and Petrology* 59:41–93.

Koch P. S. and Christie J. M. 1981. Spacing of deformation lamellae as a palaeopiezometer. *Transactions of the American Geophysical Union* 62:1030.

Landtwing M. R. and Pettke T. 2005. Relationships between SEM-cathodoluminescence response and trace-element composition of hydrothermal vein quartz. *American Mineralogist* 90:122–131.

Langenhorst F. 1994. Shock experiments on pre-heated alpha-quartz and beta-quartz: II. X-ray and TEM investigations. *Earth and Planetary Science Letters* 128:683–698.

Langenhorst F. and Deutsch A. 1994. Shock experiments on pre-heated alpha-quartz and beta-quartz: I. Optical and density data. *Earth and Planetary Science Letters* 125:407–420.

Langenhorst F. and Deutsch A. 1996. The Azuara and Rubielos structures, Spain: Twin impact craters or alpine thrust systems? TEM investigations on deformed quartz disprove shock origin (abstract). 27th Lunar and Planetary Science Conference. pp. 725–726.

Langenhorst F., Kyte F. T., and Retallack G. J. 2005. Reexamination of quartz grains from the Permian-Triassic boundary section at Graphite Peak, Antarctica (abstract #2358). 36th Annual Lunar and Planetary Science Conference: League City, Texas.

Leroux H. and Doukhan J.-C. 1993. Dynamic deformation of quartz in the landslide of Koefels, Austria. *European Journal of Mineralogy* 5:893–902.

Leroux H., Reimold W. U., and Doukhan J. C. 1994. A TEM investigation of shock metamorphism in quartz from the Vredefort Dome, South-Africa. *Tectonophysics* 230:223–239.

Lyons J. B., Officer C. B., Borella P. E., and Lahodynsky R. 1993. Planar lamellar substructures in quartz. *Earth and Planetary Science Letters* 119:431–440.

Marshall D. J. 1988. *Cathodoluminescence of geological materials*. Boston: Unwin Hyman. 146 p.

McLaren A. C., Turner R. G., Boland J. N., and Hobbs B. E. 1970. Dislocation structure of the deformation lamellae in synthetic quartz; a study by electron and optical microscopy. *Contributions to Mineralogy and Petrology* 29:104–115.

Nesse W.D. 2004. *Introduction to optical mineralogy*. Oxford: Oxford University Press, 348 p.

Officer C. B. and Carter N. L. 1991. A review of the structure, petrology, and dynamic deformation characteristics of some enigmatic terrestrial structures. *Earth Science Reviews* 30:1–49.

Okumura T., Gucsik A., Nishido H., Ninagawa K., and Toyoda S. 2009. Raman and cathodoluminescence spectroscopical microcharacterization of planar deformation features in shocked quartz from Ries impact crater (Germany). *Geological Society of America*, Abstracts with Programs, (41 No. 7): 308.

Perny B., Eberhardt P., Ramseyer K., Mullis J., and Pankrath R. 1992. Microdistribution of Al, Li, and Na in alpha quartz; possible causes and correlation with short-lived cathodoluminescence. *American Mineralogist* 77:534–544.

Poelchau M. H. and Kenkmann T. 2011. Feather features: A low-shock-pressure indicator in quartz. *Journal of Geophysical Research* 116:B02201.

Ramseyer K. and Mullis J. 1990. Factors influencing the short-lived blue cathodoluminescence of alpha-quartz. *American Mineralogist* 75:791–800.

Ramseyer K. and Mullis J. 2000. Geologic application of cathodoluminescence in silicates. In *Cathodoluminescence in Geosciences*, edited by Pagel M., Barbin V., Blanc P. and Ohnenstetter D. Berlin: Springer. pp. 177–191.

Ramseyer K., AlDahan A. A., Collini B., and Landström O. 1992. Petrological modifications in granitic rocks from the Siljan impact structure: Evidence from cathodoluminescence. *Tectonophysics* 216:195–204.

Retallack G. J., Seyedolali A., Krull E. S., Holser W. T., Ambers C. P., and Kyte F. T. 1998. Search for evidence of impact at the Permian-Triassic boundary in Antarctica and Australia. *Geology* 26:979–982.

Rusk B. and Reed M. 2002. Scanning electron microscope-cathodoluminescence analysis of quartz reveals complex growth histories in veins from the Butte porphyry copper deposit, Montana. *Geology* 30:727–730.

Rusk B. G., Reed M. H., Dilles J. H., and Kent A. J. R. 2006. Intensity of quartz cathodoluminescence and trace-element

content in quartz from the porphyry copper deposit at Butte, Montana. *American Mineralogist* 91:1300–1300.

Seyedolali A., Krinsley D. H., Boggs S., Ohara P. F., Dypvik H., and Goles G. G. 1997. Provenance interpretation of quartz by scanning electron microscope-cathodoluminescence fabric analysis. *Geology* 25:787–790.

Stevens Kalceff M. A. 2009. Cathodoluminescence microcharacterization of point defects in α-quartz. *Mineralogical Magazine* 73:585–605.

Stevens Kalceff M. A. and Phillips M. R. 1995. Cathodoluminescence microcharacterization of the defect structure of quartz. *Physical Review B* 52:3122.

Stevens Kalceff M. A., Phillips M. R., Moon A. R., and Kalceff W. 2000. Cathodoluminescence microcharacterisation of silicon dioxide polymorphs. In *Cathodoluminescence in Geosciences*, edited by Pagel M., Barbin V., Blanc P. and Ohnenstetter D. Berlin: Springer. pp. 193–224.

Stöffler D. and Langenhorst F. 1994. Shock metamorphism of quartz in nature and experiment: I. Basic observation and theory. *Meteoritics* 29:155–181.

Surenian R. 1988. Scanning electron microscope study of shock features in pumice and gneiss from köfels (Tyrol, Austria). *Geologisch-Palä ontologische Mitteilungen Innsbruck* 15:135–143.

Trepmann C. A. 2008. Shock effects in quartz: Compression versus shear deformation—An example from the Rochechouart impact structure, France. *Earth and Planetary Science Letters* 267:322–332.

Trepmann C. A. and Spray J. G. 2005. Planar microstructures and Dauphiné twins in shocked quartz from the Charlevoix impact structure, Canada. In *Large Meteorite Impacts III*, edited by Kenkmann T., Hörz F. and Deutsch A. Boulder, CO: Geological Society of America. pp. 315–328.

Trepmann C. A., Götte T., and Spray J. G. 2005. Impact-related Ca-metasomatism in crystalline target-rocks from the Charlevoix structure, Quebec, Canada. *The Canadian Mineralogist* 43:553–567.

Trukhin A. N., Jansons J. L., Dyuzheva T. I., Lityagina L. M., and Bendeliani N. A. 2003. Luminescence of different modifications of crystalline silicon dioxide: Stishovite and coesite. *Solid State Communications* 127:415–418.

Trukhin A. N., Jansons J. L., and Truhins K. 2004. Luminescence of silica glass containing aluminum oxide. *Journal of Non-Crystalline Solids* 347:80–86.

Vernooij M. G. C. and Langenhorst F. 2005. Experimental reproduction of tectonic deformation lamellae in quartz and comparison to shock-induced planar deformation features (abstract). *Meteoritics & Planetary Science* 40:1353–1361.

Vrána S. 1987. The Ševětín astrobleme, southern Bohemia, Czechoslovakia. *Geologische Rundschau* 76:505–528.

Walderhaug O. and Rykkje J. 2000. Some examples of the effect of crystallographic orientation on the cathodoluminescence colors of quartz. *Journal of Sedimentary Research* 70:545–548.

Wegner M. W. and Christie J. M. 1983. Chemical etching of deformation sub-structures in quartz. *Physics and Chemistry of Minerals* 9:67–78.

White S. H. 1973. Deformation lamellae in naturally deformed quartz. *Nature Physical Science* 245:26–28.

Williams G. E. and Gostin V. A. 2005. Acraman-Bunyeroo impact event (Ediacaran), South Australia, and environmental consequences: Twenty-five years on. *Australian Journal of Earth Sciences: An International Geoscience Journal of the Geological Society of Australia* 52:607–620.

Zinkernagel U. 1978. Cathodoluminescence of quartz and its application to sandstone petrology. *Contributions to Sedimentary Geology* 8:1–69.